PHYSICAL REVIEW B **73**, 041402(R) (2006)

Elasticity of hexagonal boron nitride: Inelastic x-ray scattering measurements

Alexey Bosak,* Jorge Serrano, and Michael Krisch
European Synchrotron Radiation Facility, Boite Postale 220, F-38043 Grenoble Cedex, France

Kenji Watanabe, Takashi Taniguchi, and Hisao Kanda
Advanced Materials Laboratory, National Institute for Materials Science, 1-1 Namiki, Tsukuba, 305-0044, Japan
(Received 15 November 2005; revised manuscript received 19 December 2005; published 19 January 2006)

The five independent elastic moduli of single-crystalline hexagonal boron nitride (*h*-BN) are determined using inelastic x-ray scattering. At room temperature the elastic moduli are in units of GPa $C_{11}=811$, $C_{12}=169$, $C_{13}=0$, $C_{33}=27.0$, and $C_{44}=7.7$. Our experimental results are compared with predictions of *ab initio* calculations and previously reported incomplete datasets. These results provide solid background for further theoretical advances and quantitative input to model elasticity in boron nitride (BN) nanotubes.

DOI: 10.1103/PhysRevB.73.041402 PACS number(s): 62.20.Dc, 61.10.Eq, 63.20.Dj

The physical and chemical properties of boron nitride (BN) have been extensively studied in the past years. Among the many polymorphs of BN, graphitelike hexagonal boron nitride (*h*-BN) with (AA) layers stacking, is one of the most common. It is stable in a suitable atmosphere up to 2800 °C, chemically inert, a good thermal conductor and electric insulator, and it is easy to machine. Hexagonal BN finds applications as a high-temperature lubricant, as a heat sink or substrate in electronic devices, and in the production of ceramic parts and coatings.[1] Furthermore, it was recently[2] shown that *h*-BN has a direct band gap of 5.97 eV and provides ultraviolet lasing at 215 nm, opening the possibility for the development of compact ultraviolet lasers to be used for optical storage, photocatalysis, and in medical applications.

Despite the undoubted scientific and technological relevance of *h*-BN experimental results on vibrational and elastic properties, using Raman spectroscopy[3,4] and high-resolution electron energy loss spectroscopy[5] are scarce or incomplete. More specifically, elasticity data available until now were obtained on pyrolytic *h*-BN samples by ultrasound measurements[6] and indirectly from thermal conductivity data.[7] Results on pyrolytic samples are widely scattered since their properties are linked to the defect structure, the size of ordered grains, and the interlayer connectivity. For example, the value of the shear elastic modulus C_{44} can vary by two orders of magnitude as a function of sample morphology.[7] It has now become possible to grow single crystals of good quality by high-pressure/high-temperature synthesis in a Ba–B–N catalyst system,[2,8] thus overcoming the above-mentioned limitations and opening the possibility to obtain reliable elasticity data.

In this paper we present the experimental determination of the five independent elastic moduli of single-crystalline *h*-BN using inelastic x-ray scattering (IXS). The moduli are obtained via the sound velocities V as derived from the initial slope of the acoustic phonon branches along specific, mostly high-symmetry, directions, and Christoffel's equation.[9] The IXS experiment was performed on beamline ID28 at the European Synchrotron Radiation Facility. The instrument was operated at 17794 eV and provided an overall energy resolution of 3.0 meV FWHM. The dimensions of the focused x-ray beam were 250×60 μm^2 (horizontal $\times$ vertical FWHM). The direction and size of the momentum transfer were selected by an appropriate choice of the scattering angle and the sample orientation in the horizontal scattering plane. The momentum resolution was set to 0.2 nm^{-1} and 0.7 nm^{-1} in the horizontal and vertical plane, respectively. Further details of the experimental setup can be found elsewhere.[10] The investigated *h*-BN single crystals were platelets with a typical size of 0.6–1.0 mm in the *a*-*b* plane and 50 to 120 μm along the *c* axis. The crystals were of good crystalline quality as evidenced by a rocking curve width of only 0.025° FWHM [measured on the (1 1 0) reflection], and the determined lattice parameters $a=2.506$ Å, $c=6.657$ Å are in excellent agreement with previous x-ray diffraction results $a=2.504$ Å, $c=6.660$ Å.[11]

In Fig. 1 we report examples of the collected IXS spectra. These are characterized by an elastic contribution centered at zero energy and two symmetric features, the Stokes and anti-Stokes peaks of the BN acoustic phonons. The energy position $E(q)$ of the phonons was extracted using a model function composed of a sum of Lorentzian functions for which the inelastic contributions were constrained by the Bose factor. This model function was convoluted with the experimentally determined resolution function and fitted to the IXS spectra utilizing a standard χ^2 minimization routine. Typically, two to five IXS spectra were recorded along a specific crystallographic direction. The sound velocity is derived from the slope of the acoustic phonon dispersion in the low q limit, in most cases by a linear or a sinusoidal fit $E(q)=A\cdot\sin(\pi q/B)$, formally equivalent to limiting the interatomic interactions to nearest neighbors. However, due to the layered nature of *h*-BN and consequently the high elastic anisotropy, the transverse acoustic phonon branch along [1 1 0] with *c*-axis polarization $TA[110]_{\langle 001\rangle}$ (here and below, the polarization vector is indicated as a subscript) displays a parabolic dispersion at low q: $\omega^2=Cq^2+Dq^4$, and the slope at $q=0$ is given by $\sqrt{C}$.[12]

A further consequence of the high anisotropy of *h*-BN is the need to take into account the effect of the finite resolution in momentum transfer q defined by the angular opening of the analyzers. In the proximity of the Γ point the spread in $|\vec{q}|$ can usually be ignored whereas the directional spread can become significant, in particular in the proximity of special points on constant-$|\vec{q}|$ surfaces. This is illustrated in Fig. 2 for

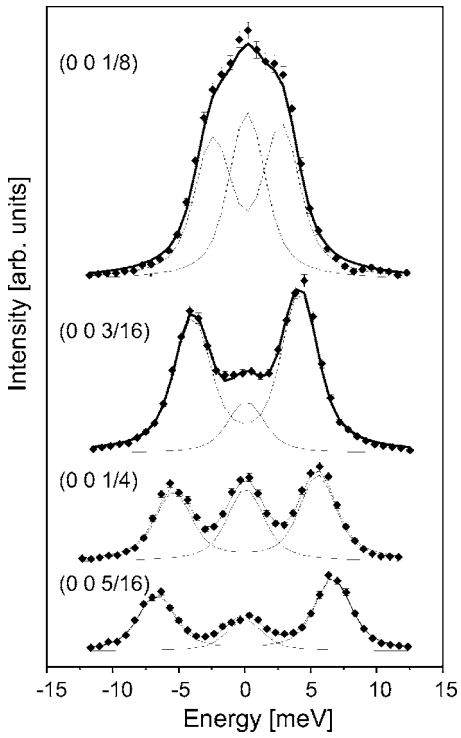

FIG. 1. Selected IXS spectra for the TA[0 0 1] branch at the indicated q values (given in reciprocal lattice vector components). The experimental data are shown together with the best fit results (thin solid lines for the individual components and solid lines for the total fit). The spectra are shifted in the vertical direction for clarity, conserving the same intensity scale. The counting time per point was 1 min.

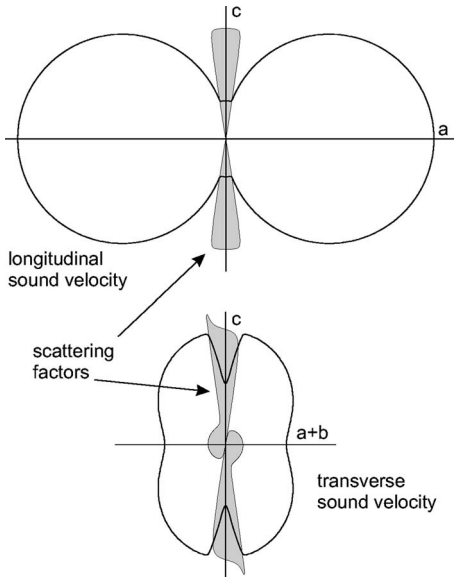

FIG. 2. Polar plots of the longitudinal and transverse sound velocities with approximate inelastic x-ray scattering factors, calculated in the low-q limit around (0 0 2) and (1 1 2) Bragg reflections, respectively. The polarization vector of transverse sound waves lies in the plane of the drawing defined by the ⟨001⟩ and ⟨110⟩ directions.

the longitudinal (LA) [0 0 1] and transverse (TA) [0 0 1] sound velocities recorded around the (0 0 2) and (1 1 2) Bragg spots, respectively, where the angular spreads are close to each other and can attain 20° for one of the directions. Polar plots of LA and TA sound velocities are shown together with the approximate IXS scattering factors $S_j(\theta)$ calculated in the low-q limit: $S_j(\theta) \propto |\hat{e}_j(\theta) \cdot \vec{Q}|^2$. Here, $\hat{e}_j(\theta)$ denotes the phonon polarization vector and θ the angle with respect to the basal a-b plane. The momentum transfer $\vec{Q}$ ($\vec{Q}=\vec{q}+\vec{\tau}$, $\vec{q}$–reduced momentum transfer vector, $\vec{\tau}$–nearest reciprocal lattice vector) is directed towards the corresponding Γ point, (0 0 2) and (1 1 2) for the LA and the TA branch, respectively. While the correction for the longitudinal sound velocity is less than 0.2%, for the transverse sound velocity the correction amounts to 40%.

Table I provides the list of the investigated phonon branches and the corresponding derived sound velocities. This choice of directions allows one to obtain all five independent elastic moduli. Apart from C_{13} all other elastic moduli can be calculated directly from a single sound veloc-

TABLE I. Summary of the investigated acoustic branches, indicating the direction of the total momentum transfer Q, the propagation and polarization vector of the phonon, and the derived apparent sound velocity. The parameter ξ is always positive; polarization vectors for quasi-longitudinal (q-LA) and quasi-transverse (q-TA) phonon branches are not indicated.

Notation	Momentum transfer	Propagation vector	Polarisation vector	Velocity (km/s)
LA[1 0 0]	[1+ξ 0 0]	[1 0 0]	⟨1 0 0⟩	18.86(14)
TA[1 0 0]$_{\langle 1-20\rangle}$	[1 ξ 0]	[1 0 0]	⟨1 −2 0⟩	11.86(12)
TA[1 1 0]$_{\langle 1-10\rangle}$	[1−ξ 2ξ 0]	[1 1 0]	⟨1 −1 0⟩	
TA[1 1 0]$_{\langle 001\rangle}$	[1−ξ 1−ξ 2]	[1 1 0]	⟨0 0 1⟩	1.84(6)
LA[0 0 1]	[0 0 2+ξ]	[0 0 1]	⟨0 0 1⟩	3.44(3)
TA[0 0 1]	[1 1 2−ξ]	[0 0 1]	⟨1 1 0⟩	2.57(6)
q-TA[1 1 2]	[1−ξ 1−ξ 2−2ξ]	[1 1 2]		2.10(2)
q-LA[1 1 30]	[1−ξ 1−ξ2+30ξ]	[1 1 30]		3.71(4)
q-TA[1 1 36]	[1−ξ 1−ξ 2+36ξ]	[1 1 36]		3.23(4)

TABLE II. Comparison of our results with previous experiments and calculations. All values are in GPa.

	C_{11}	C_{12}	C_{13}	C_{33}	C_{44}	B
present exp.	811(12)	169(24)	0(3)	27.0(5)	7.7(5)	25.6(8)
other exp.[6,7,11]	750[6]	150[6]	—	32[6]	3[7]	36.7[11]
theory (Green *et al.*)[16]	802.5	267.5	3.0	31.2	3.0	29.8
theory (Ohba *et al.*)[17]	951.5	169.2	2.5	28.2	—	27.07

ity, i.e., $C_{11}=\rho V(\mathrm{LA}[100])^2$, $C_{66}=\rho V(\mathrm{TA}[100]_{\langle 1-20\rangle})^2$, $C_{44}=\rho V(\mathrm{TA}[110]_{\langle 001\rangle})^2=\rho V(\mathrm{TA}[001])^2$, $C_{33}=\rho V(\mathrm{LA}[001])^2$, where ρ is the density. C_{13} contributes to the sound velocity only for nonpure directions (*i.e.*, those neither in the equatorial plane nor along the axial direction). Based on the results for C_{11}, C_{66}, C_{44}, and C_{33}, the most favorable direction with largest $|dV/dC_{13}|$ occurs for $\theta\sim 10$ deg, and the phonon dispersion was therefore determined along the $\langle 1\ 1\ 36\rangle$ and $\langle 1\ 1\ 30\rangle$ directions. Corresponding Bragg spots were chosen among the strongest ones accessible within the geometrical constraints of the experimental setup.

The sound velocities could be derived with an error of about 1–3%. The apparent sound velocity determined from the TA[0 0 1] branch has to be corrected, as discussed above, by 40%. The obtained value of 1.84 km/s is in perfect accordance with our value for $\mathrm{TA}[1\ 1\ 0]_{\langle 001\rangle}$.

The set of elastic moduli calculated in a self-consistent manner on the basis of our experimental observations is given in Table II, and the fitted sound velocities are presented in a polar plot in Fig. 3. C_{13} is poorly defined due to the very large structural anisotropy, but we can conclude that it is very close to zero. Comparison with C_{13} of graphite is not possible, as published values vary from −51 to 22 GPa.[13,14] In-plane elastic moduli are significantly larger than those obtained by ultrasonic measurements, most likely due to the much higher disorder in pyrolythic *h*-BN samples. The difference is even larger for C_{44}, which is linked with interlayer bonding and is strongly dependent on sample preparation conditions.

The only available value for the bulk modulus was obtained by x-ray diffraction from a polycrystalline sample[11] and is significantly higher than both theoretical predictions and our result. As the bulk modulus is defined for constant stress throughout the body, this corresponds to the Reuss approximation in polycrystals, where boundary conditions for the strain are neglected. The interaction between grains can significantly increase the value of the experimentally determined bulk modulus. For *h*-BN the upper limit of the bulk modulus for a compact (isotrope) aggregate is around 100 GPa if calculated in a self-consistent scheme[15] obeying $\langle C\rangle=\langle C^{-1}\rangle^{-1}$; thus, these data cannot be considered as contradictory.

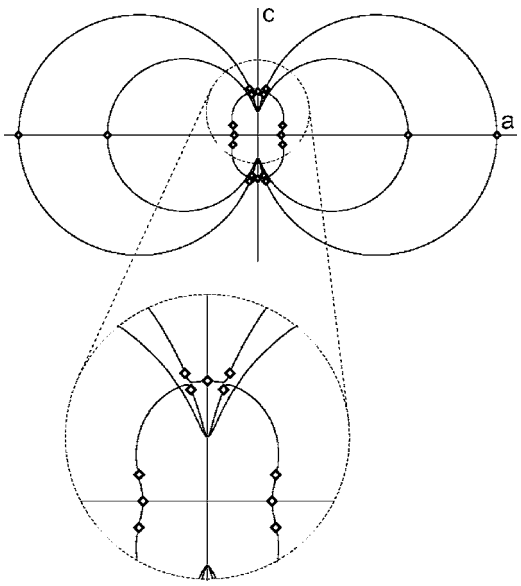

FIG. 3. Polar plot of the derived sound velocity data in the a–c plane: experimental data (diamonds), solid lines (fit results). The low-velocity part is shown enlarged on the bottom.

The first attempt to calculate the elastic behavior of BN used a central force model[16] (Lennard–Jones potential and electrostatic part), which gave a reasonable description despite model constraints (i.e., $C_{13}=C_{44}$, $C_{11}=3C_{12}$). *Ab initio* calculations employing ultrasoft pseudopotentials and density functional perturbation theory[17] assure much better agreement for all the elastic moduli except C_{11} and $C_{66}=(C_{11}-C_{12})/2$. As our elastic moduli can be considered as the upper bound for *h*-BN, they provide solid background for further theoretical advances.

Finally, it is important to note that our value of C_{11} provides the upper estimate of the on-axis Young's modulus of a homogeneous BN nanotube. These tubes are currently the subject of intense research efforts for applications as high-strength non-conducting fibers. Contrary to carbon nanotubes, direct measurements are scarce, and the obtained value of 1.22 ± 0.24 TPa[18], compared to our value of 811 GPa for C_{11}, seems to be much too large.

The authors would like to thank L. Wurtz and A. Rubio for fruitful discussions and for sharing their results on calculated elastic moduli.

*Electronic address: bossak@esrf.fr

[1] R. Haubner, M. Wilhelm, R. Weissenbacher, and B. Lux, *Boron Nitrides—Properties, Synthesis and Applications, in Structure and Bonding* (Springer-Verlag, Berlin, 2002), Vol. 102.

[2] K. Watanabe, T. Taniguchi, and H. Kanda, Nat. Mater. **3**, 404 (2004).

[3] R. Geick, C. H. Perry, and G. Rupprecht, Phys. Rev. **146**, 543 (1966).

[4] T. Kuzuba, K. Era, T. Ishii, and T. Sato, Solid State Commun. **25**, 863 (1978).
[5] E. Rokuta, Y. Hasegawa, K. Suzuki, Y. Gamou, C. Oshima, and A. Nagashima, Phys. Rev. Lett. **79**, 4609 (1997).
[6] B. Jager, PhD thesis, Université de Grenoble, Grenoble, 1977 (in French).
[7] L. Duclaux, B. Nysten, J.-P. Issi, and A. W. Moore, Phys. Rev. B **46**, 3362 (1992).
[8] T. Taniguchi and S. Yamaoka, J. Cryst. Growth **222**, 549 (2001).
[9] B. A. Auld, *Acoustic Fields and Waves in Solids* (J. Wiley and Sons, New York, 1973), Vol. 1.
[10] M. Krisch, J. Raman Spectrosc. **34**, 628 (2003).
[11] V. L. Solozhenko, G. Will, and F. Elf, Solid State Commun. **96**, 1 (1995).
[12] H. Zabel, J. Phys.: Condens. Matter **13**, 7679 (2001).
[13] O. L. Blakslee, D. G. Proctor, E. J. Seldin, G. B. Spence, and T. Weng, J. Appl. Phys. **41**, 3373 (1970).
[14] H. J. F. Jansen and A. J. Freeman, Phys. Rev. B **35**, 8207 (1987).
[15] S. Matthies and M. Humbert, J. Appl. Crystallogr. **28**, 254 (1995).
[16] J. F. Green, T. K. Bolland, and J. W. Bolland, J. Chem. Phys. **64**, 656 (1976).
[17] N. Ohba, K. Miwa, N. Nagasako, and A. Fukumoto, Phys. Rev. B **63**, 115207 (2001).
[18] N. G. Chopra and A. Zettl, Solid State Commun. **105**, 297 (1998).